Text: Featuring research from Dr Shi Cheng and Dr Zhigang Wu at the Uppsala University, The Ångström Laboratory, Uppsala, Sweden.

Title: Microfluidic stretchable RF electronics

Microfluidic stretchable integrated radiofrequency electronics showcases a revolutionary technology for electronics and microfluidics societies, which potentially create a world of radically different electronic devices and systems that open up an entirely new spectrum of possibilities.

As featured in:

See Cheng and Wu, *Lab Chip*, 2010, **10**, 3227.

RSC Publishing

www.rsc.org/loc

Registered Charity Number 207890

Microfluidic stretchable RF electronics†

Shi Cheng and Zhigang Wu*

Received 20th April 2010, Accepted 27th August 2010
DOI: 10.1039/c005159d

Stretchable electronics is a revolutionary technology that will potentially create a world of radically different electronic devices and systems that open up an entirely new spectrum of possibilities. This article proposes a microfluidic based solution for stretchable radio frequency (RF) electronics, using hybrid integration of active circuits assembled on flex foils and liquid alloy passive structures embedded in elastic substrates, *e.g.* polydimethylsiloxane (PDMS). This concept was employed to implement a 900 MHz stretchable RF radiation sensor, consisting of a large area elastic antenna and a cluster of conventional rigid components for RF power detection. The integrated radiation sensor except the power supply was fully embedded in a thin elastomeric substrate. Good electrical performance of the standalone stretchable antenna as well as the RF power detection sub-module was verified by experiments. The sensor successfully detected the RF radiation over 5 m distance in the system demonstration. Experiments on two-dimensional (2D) stretching up to 15%, folding and twisting of the demonstrated sensor were also carried out. Despite the integrated device was severely deformed, no failure in RF radiation sensing was observed in the tests. This technique illuminates a promising route of realizing stretchable and foldable large area integrated RF electronics that are of great interest to a variety of applications like wearable computing, health monitoring, medical diagnostics, and curvilinear electronics.

1 Introduction

During the past two decades, remarkable progress mainly driven by biological and medical applications has been made in the microfluidics society.[1–3] However, potential applications of microfluidics in other fields have seldom been exploited. As one of the fastest growing areas in industry sector, electronics industry generates billions of Dollars and Euros profits every year. Successful use of microfluidic techniques in electronics[4] will not only open up a brand-new research area for the microfluidics society, but also bring large amounts of benefits to the microfluidics and electronics industries. The marriage of microfluidics and electronics may offer effective solutions for specific application scenarios, in which conventional electronics are impossible to fulfil the requirements.[5–11]

Large area electronics with a high degree of flexibility and stretchability, so-called stretchable electronics have been recently proposed and explored.[12–14] In contrast to microelectronics and nanoelectronics aiming at developing smaller and faster devices, stretchable electronics can be made in the form of distributing yet integrating microelectronic devices over large area elastic substrates with sizes much larger than semiconductor components.[15–17] This kind of electronics is favoured in applications like body-worn wireless sensor nodes,[18] radio frequency identifications (RFIDs), and conformable skins for integrated robotic sensors to enhance the comfort for the users and make the installation on curved interfaces easier.[17] Since conventional materials for electronics manufacturing are rigid, the demands for electronic devices that can flex, stretch, or reach extreme levels of folding challenge the standard material and processing technologies.

Various approaches to implement stretchable large area electronics have been presented by several research groups. Foldable and stretchable silicon integrated circuits (ICs) on "wavy" silicon ribbons on silicone rubber substrates were first proposed by Rogers *et al.* for fully integrated stretchable electronics.[19,20] Further, interesting prototypes such as wearable electronics,[21] artificial eyes,[22] and implanted medical devices[23] have been demonstrated. From technical perspective, this technology is so far the most promising solution for high performance stretchable electronic devices as it allows densely distributed active electronics with high precision as well as high degrees of elasticity. The fact of massive consumption of silicon on insulator (SOI) wafers may however hinder the use of this technology in consumer electronics because of the considerable material cost for large area devices with sizes of tens of square centimetres. Alternative solution is to incorporate stretchable interconnects and thin film transistor (TFT) circuits on pre-strained elastomeric substrates.[24,25] Stretchable meandered passive interconnects with a longitudinal elongation up to 20% were shown at high frequencies for the first time.[26–28] Nevertheless, stretchability, especially along multi-axis, is still restricted by the mechanical mismatch between the solid metals and elastic materials in these approaches. Advanced nano-materials such as self-assembled nanocomposite materials and single-walled carbon nanotube (SWNT) conductors have been demonstrated with attractive mechanical characteristics,[29] *e.g.* uniform elasticity and extreme levels of foldability. But the relatively high sheet resistance of these materials compared to conventional metals results in significant increase in conductive losses. The above mentioned studies deal with either low-frequency ICs or

Department of Engineering Sciences, Uppsala University, The Angstrom Laboratory, Box-534, SE-751 21 Uppsala, Sweden. E-mail: Zhigang.Wu@angstrom.uu.se

† Electronic supplementary information (ESI) available: Additional data. See DOI: 10.1039/c005159d

relatively simple interconnects. Stretchable integrated electronic devices at radio frequencies have not been reported up to date. Is it possible to seek for a cost-effective approach to implement stretchable integrated electronics at high frequencies?

Microfluidics might offer a promising solution for stretchable large area electronics at an affordable cost. It is well-known that microstructured elastomeric channels are widely used in microfluidic devices. What if such elastic channels are filled with highly conductive liquid and used as wires for conducting electronic signals? The possibility of implementing microfluidic electronics was first investigated by Whitesides *et al.* using low temperature melting solder.[5,6] Multi-axially stretchable DC interconnects by filling elastomeric channels with eutectic Gallium and Indium alloy were also reported.[7,8] Recently, the first high-performance stretchable antennas based on Galinstan filled microfluidic channels were demonstrated by Cheng *et al.*[9,10] Later, another type of elastic liquid metal antenna was presented using eutectic Gallium and Indium alloy.[11] The successful demonstration of stretchable antennas paves the way for realizing stretchable RF electronic devices that provide attractive functionality, for instance, wireless communications and remote sensing. Nevertheless, due to the absence of semiconductor components like transistors and diodes in microfluidic manufacturing processes, monolithic integration of active electronic systems is infeasible so far.

This paper proposes a cost-effective hybrid approach for integrating conventional rigid active electronics to microfluidic stretchable passive components at radio frequencies. Stiff cells encapsulating active circuits on flexible laminates are employed to ensure reliable interfaces between non-stretchable active circuits and stretchable passive parts. Based on the proposed concept, a 900 MHz integrated stretchable RF radiation sensor with a lighting-emitting diode (LED) acting as an indicator was implemented and evaluated. In addition to integration approaches, system designs, and fabrication processes, experimental results on mechanical and electrical characteristics of the standalone antenna, the RF power detection sub-module as well as the integrated RF radiation sensor are also addressed in this article.

2 Principles and system design

Feasibilities of implementing standalone stretchable antennas based on microfluidic techniques have been proven.[9–11] But essential semiconductor components such as transistors and diodes are impossible to directly produce using existing microfluidic technologies. This bottleneck hinders monolithic integration of microfluidic electronic systems containing active circuits. However, this issue can be circumvented to some extent, with a compromising solution, in which conventional semiconductor components are distributed over large area elastic substrates and interconnected with liquid alloy filled stretchable channels. Owing to advances in modern semiconductor processes, extremely high integration densities can be achieved, with more and more functionality integrated into miniaturized IC chips or packages. When miniaturized ICs are distributed over large area stretchable substrates at a relatively low density, mechanical properties, *e.g.* stretchability and foldability, of the entire devices will not be significantly degraded.

The remaining major issue is how to produce reliable interfaces between rigid ICs and stretchable passive sub-modules. Commercially available ICs are usually packaged with a number of protruding metallic contacts. A trivial solution would be to directly plug those contact pins into the openings of microfluidic channels and dip them into the liquid alloy. It is feasible for relatively simple ICs or components with limited numbers of interconnects. For complex devices containing dozens of ICs modules with tens or even hundreds of contacts each, producing thousands of such interconnects with good yield must be a real challenge. Another issue that should be taken into account is the mechanical mismatch between rigid components and elastic structures. This may degrade the reliability of the entire devices during straining or folding. Accordingly, a new method of connecting rigid components to liquid alloy filled elastic channels is required.

2.1 Hybrid integration of stretchable antenna and flexible active circuitry

Flexible printed circuits (FPCs), using very thin soft dielectric and metal layers, are extensively used in consumer electronics. The processes of assembling large numbers of complex ICs and passive components on flex foils are mature and reliable. Although their flexibility is very limited and certainly not intended to be stretched or twisted, devices containing a few miniaturized flexible circuits sparsely distributed over large area elastic substrates can still achieve certain degrees of stretchability and foldability. This concept enables complex routing implemented on flex foils instead of using elastic microfluidic interconnects, and eliminates unreliable rigid-to-stretch interfaces. In this case, only small amounts of interconnects between FPCs and stretchable sub-modules are needed for a complex integrated device. Furthermore, compared to the rigid-to-stretch interconnects, the interfaces between flex foils and elastic parts feature lower mechanical mismatches, and should be able to tolerate higher mechanical stress.

FPCs are not made for stretching or twisting and thus set an upper limit for the elasticity of integrated devices. In order to enhance the overall stretchability of an integrated device, the stress in the areas of flexible circuits should be minimized. One feasible solution is to introduce localized stiff cells (LSCs) by locally thickening and stiffening the elastic substrate. Due to the inverse proportion of the stress and thickness of elastic materials, the stress in the LSCs is lower than that in other areas of the strained substrate. Hence, miniaturized flexible circuits together with flex-to-stretch interfaces embedded in such LSCs can be isolated to a certain extent from intense stress distributed over other parts of the substrate.

Unlike highly miniaturized ICs, miniaturization of antennas can only be achieved at the expense of poor electrical performance, due to the fundamental limitations imposed by the physics. To maintain reasonable RF performance, the key components, antennas, in wireless communication or remote sensing devices, must be made relatively larger than other electronics, and hence dominate the overall mechanical characteristics of the integrated devices. As illustrated in Fig. 1, a large antenna is thereby made in the highly stretchable and foldable format, by incorporating liquid alloy into microstructured elastic

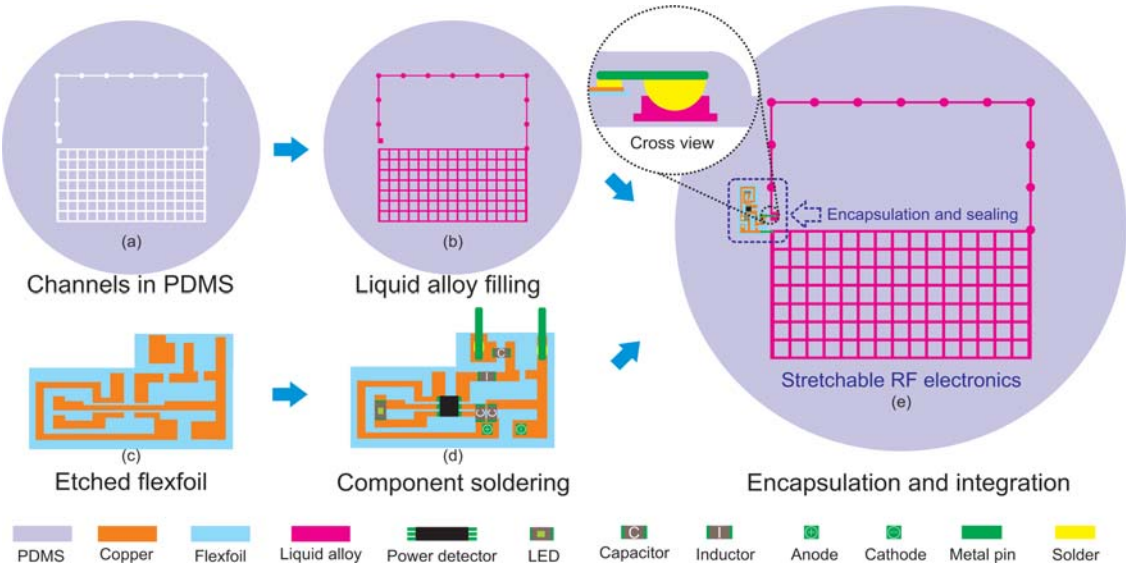

Fig. 1 Schematic of the proposed integration concept for stretchable RF electronics.

channels, whereas conventional ICs and passive components are assembled on small pieces of flexible laminates. Subsequently, several tin-plated contact pins resembling cantilevers are soldered to the FPCs. On the other end of each contact pin, a semi-spherical solder ball is mounted on the bottom surface for improving electrical connection to the liquid alloy in microfluidic channels, *cf.* Fig. 1(e). Whereafter, the FPCs are embedded into the antenna substrate, where each contact pin is plug into an opening of the channel and dipped into the liquid alloy. Lastly, uncured PDMS droplets are poured on top of the FPCs to locally thicken the elastic substrate and encapsulate the flexible circuits as well as the flex-to-stretch interfaces. Because of the much higher stiffness of these LSCs than other areas, nearly zero stress and displacement between the rigid and stretchable structures arise inside the LSCs even though the entire device is severely strained. Compared to the standalone elastic antenna, the overall elasticity of the integrated device will be degraded due to the presence of the LSCs, but the reliability of the entire system is enhanced. Moreover, good wetting of the chosen liquid alloy on tin-plated pins and solder balls ensures reliable electrical connections between the contact pins and the antenna.

2.2 System design

To verify the proposed concept, a 900 MHz microfluidic stretchable RF radiation sensor was designed, implemented, and tested. The presented sensor is capable of performing on-going measurements of the human exposure level to electromagnetic fields (EMF) in the environment. In case of high exposure level to EMFs that may be harmful to the human health, a warning signal will be sent out. This sensor device is of importance to the human health as the increasing EMFs generated by more and more modern wireless communication systems might cause the health issues. The schematic of the application scenario is shown in Fig. 2. The demonstrated sensor was composed of three sub-modules fully embedded in a large area elastic substrate: a stretchable unbalanced loop antenna for receiving RF radiation from free space, a RF power detection sub-module for converting received RF power to the corresponding DC voltages, and a LED indicator for visualizing the RF radiation sensing. In addition to those integrated modules, an external DC power supply was required for powering the active circuits in the RF radiation sensor. In the system demonstration, the RF radiation source containing a horn antenna with its co-polarization vertically aligned and a RF signal generator was placed at a distance of a few meters from the RF radiation sensor.

3 Material and methods

3.1 Materials and chemicals

The PDMS Kit, Elastosil RT601A and B from Wacker Chemie (München, Germany) was employed for fabricating the elastomeric substrates. The SU-8 2050 as well as the developer from MicroChem (MA, US) was used for manufacturing the master on a 6-inch silicon wafer from Wacker Chemie. The room temperature liquid alloy, Galinstan was from Geratherm medical AG (Geschwenda, Germany). The positive photoresist, Shipley 1813 as well as the developer from MicroChem was utilized for the FPC fabrication. The 50 μm thick flexible polyimide substrates with 17 μm thick copper layer on single side were from

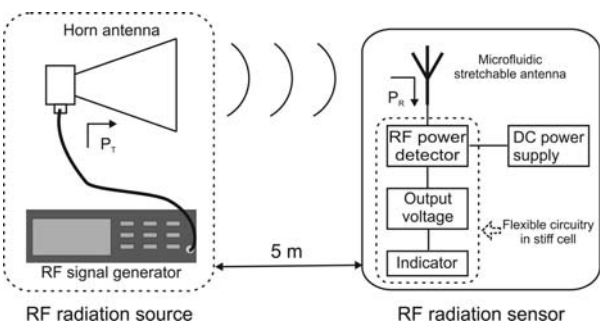

Fig. 2 Schematic of the RF radiation sensing demonstration setup.

Dupont (Wilmington, Delaware, USA). Surface mount components including RF power detector 50MHz-3GHz, SC70-6, 0805 capacitors, 0402 inductors, and 0805 green LEDs from Farnell (Malmö, Sweden) were assembled to the flex foils using the solder paste (CR 44 SMD Lotpaste) from Farnell. Duracell® AA size NIMH rechargeable batteries were from a local electronic store. All the solvents, such as acetone, ethanol alcohol, isopropanol (IPA), used in the fabrication processes were from VWR international (Stockholm, Sweden).

3.2 Device fabrication and integration

The fabrication steps of microfluidic stretchable antennas have been previously described in detail.[10] In brief, the patterns of the antenna were transferred to a 75 μm thick negative photoresist SU-8 on a 6 inch silicon wafer (master) using a transparency mask. The microstructured channel networks in the PDMS substrate were then constructed by replicating the SU-8 patterns on the master. Afterwards a couple of holes were punched out for liquid alloy injection and RF connection. A blank PDMS lid was then bonded onto the thin PDMS replica. Through the punched holes in the PDMS, the liquid alloy was manually injected into the microfluidic channels. The ventilation outlets were encapsulated with uncured PDMS mixture in the end.

The FPCs were fabricated using standard printed circuit board (PCB) manufacturing processes. Approximately 1 μm thick positive photoresist was spun on the top metallization of a flex foil and baked at 105 °C for 75 S. The patterns of the RF power detection circuits were then transferred to the top copper layer, *via* UV exposure, soft bake, developing, and hard bake. After depositing solder paste droplets on the patterned copper layer, ICs as well as passive components for RF power detection were manually placed on the flex foil. Subsequently, the flex foil together with the mounted components were heated at 220 °C for 2 min in a convective oven and cooled down at room temperature. Finally, two metallic pins perpendicular to the flex foil for external DC power supply were soldered.

Prior to the final integration, electrical performance of the standalone antenna and the RF power detection sub-module were experimentally evaluated as described in the following section. As presented in the previous section, two contact pins for connecting the RF power detector to the elastic antenna were respectively soldered to the RF signal and ground ports of the detector. The detector sub-module was then integrated to the elastic antenna with each pin directly contacting the liquid alloy. The circuits on the flexible laminate and the two contact pins were encapsulated in a LSC by locally depositing and curing uncured PDMS mixture. The integrated microfluidic stretchable RF radiation sensor is shown in Fig. 3.

3.3 Antenna and circuitry characteristics

The detailed design and measurement procedures of the liquid metal stretchable antennas have been reported elsewhere.[9,10] As described in Fig. S1, ESI,‡ the overall length of the upper antenna arm corresponds to approximately a half of the effective wavelength at the frequency of operation. Prior to experiments, the non-stretched antenna with an original size of 88.0 mm × 86.9 mm was numerically analyzed in full-wave simulations using

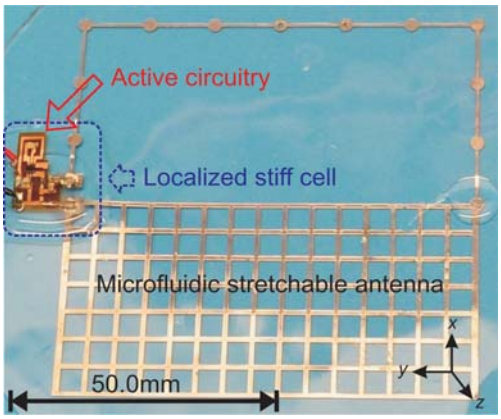

Fig. 3 Photograph of the demonstrated stretchable RF radiation sensor.

Ansoft HFSS. Port impedance and radiation efficiency of both the non-strained and strained antennas were characterized using a network analyzer (Agilent Technologies E8364B, PNA series) in ordinary lab environment and a large reverberation chamber, respectively. Later, the radiation patterns were measured in an anechoic chamber, using an Agilent E4440A PSA Series Spectrum Analyzer, a Keithley 2910A RF Signal generator, a motor controlled turntable, and a double ridge guide horn antenna, SAS-571 (A.H. Systems, Inc.).

The active circuitry of the demonstrated RF radiation sensor consists of a RF power detector (Linear Technology, LT 5534), two decoupling capacitors (C_2 and C_3), a coupling capacitor (C_1), an inductor (L_1) for impedance matching at the RF input port, and a green LED indicator. All the above mentioned components were assembled on a flex foil with a size of 10 mm × 18 mm, *cf*. Fig. S2, ESI.‡ The RF power detector was chosen for its appropriate RF power detection range around 900 MHz. When sufficient RF power was injected into the detector, the LED indicator would be switched on, and *vice versa*. The entire RF power detection sub-module was powered by four serially connected AA rechargeable batteries with a DC supply voltage of 5.23 V. In the active circuitry characterizations, the LED was firstly removed and the output of the RF power detector (V_{OUT}) was directly connected to a Keithley 197A autoranging microvolt digital multimeter. The RF input of the power detection circuits was connected to a signal generator Anritsu MG 3694A *via* a tunable HP 8495A attenuator. By adjusting the output power level of the 900 MHz continuous wave (CW) at the signal generator and the insertion loss of the attenuator, the corresponding DC output voltages *versus* varying input RF power (P_R) were measured at the digital multimeter. After that the digital multimeter connected to the DC output of the RF power detector was replaced by a LED, and its on/off states with different input RF power levels were recorded. The DC power consumption of the entire power detection module at a DC supply voltage of 5.23 V was finally measured using a Keithley 236 source measure unit.

3.4 Integrated device demonstration

The integrated stretchable RF radiation sensor was tested in a demonstration setup illustrated in Fig. 2. The RF radiation

source is composed of a RF signal generator and a horn antenna illuminating the stretchable RF radiation sensor placed 5 m away. The RF power injected into the horn antenna was set to 20 dBm and the antenna gain is around 7.4 dBi. Experiments on verifying the radiation sensing functionality of the mechanically deformed sensor were first performed in ordinary office environment. For comparison, the same experiments were also conducted in an anechoic chamber afterwards.

4 Results and discussion

4.1 Antenna performance

Good port impedance matching at 900 MHz as well as excellent agreements between the simulated and measured reflection coefficients (S_{11}) of the non-stretched antenna are seen in Fig. S3, ESI.‡ While the antenna was strained along either *x*- or *y*-axis, resonance frequency decrease was observed as shown in Fig. 4. This was mainly due to the increased antenna size during stretching. The measured antenna radiation efficiency at 900 MHz is presented in Table 1. Benefiting from high conductivity of the liquid metal alloy ($\sigma = 3.46 \times 10^6$ S/m)[32] and relatively large cross dimensions of the microfluidic channels, low conductive loss and high radiation efficiency of the antenna could be expected. As shown in Table 1, a radiation efficiency of higher than 80% was achieved even if the antenna was stretched to 15%, which was better than most internal antennas in mobile handsets. It is known that PDMS is not a favourable dielectric material at microwave frequencies because of its high dielectric losses and uncertain relative permittivity. The reason for the high radiation efficiency of the presented antenna was the negligible influence of the very thin PDMS substrate, whose thickness was approximately 1/300 wavelength around 900 MHz.

The antenna featured slightly lower radiation efficiency with greater elongation due to the larger resonance frequency shift. Simulated and measured radiation patterns of the non-stretched and stretched antennas at 900 MHz are presented in Fig. S4, ESI.‡ Similar to conventional unbalanced loop antennas, the non-strained antenna exhibited very broad coverage, especially in the *yz*-plane where almost perfect omnidirectionality was achieved. This feature is favoured in various applications, *e.g.* mobile terminals and wireless sensor nodes. The maximum antenna gain was found to be around 2.7 dBi. The cross-polarization discrimination was very good, something which also verified the low disturbances from the measurement setup. Stretching the antenna along either *x*- or *y*-axis up to 15% introduced slight variations in the measured radiation patterns. No significant gain reduction or omnidirectionality degradation could however be observed. The results imply that electrical connections in the microfluidic channels were not interrupted by straining and folding. This owed to excellent wetting between the liquid alloy and the surfaces of the elastic channels. However, according to some previous studies,[30–32] Gallium or Galinstan is easy to oxidize in air at room temperature, and the thin oxidization layers may affect its rheological properties and wettablity on PDMS surfaces. Furthermore, the breathing properties of PDMS might lead to crucial issues on the oxidization of the liquid alloy. The long-term characteristics of liquid alloy filled microfluidic channels should thereby be investigated later.

Table 1 Measured radiation efficiency at 900 MHz of the stretched and non-stretched antennas

Elongation	Radiation efficiency
Non-stretched	94%[a]
5% *x*-axis	92%
10% *x*-axis	89%
15% *x*-axis	87%
5% *y*-axis	84%
10% *y*-axis	83%
15% *y*-axis	81%

[a] Simulated radiation efficiency of the non-strained antenna is 95%.

4.2 Electronic circuitry performance

The standalone RF power detection sub-module was characterized by applying varying RF power at its input. Fig. 5 presents

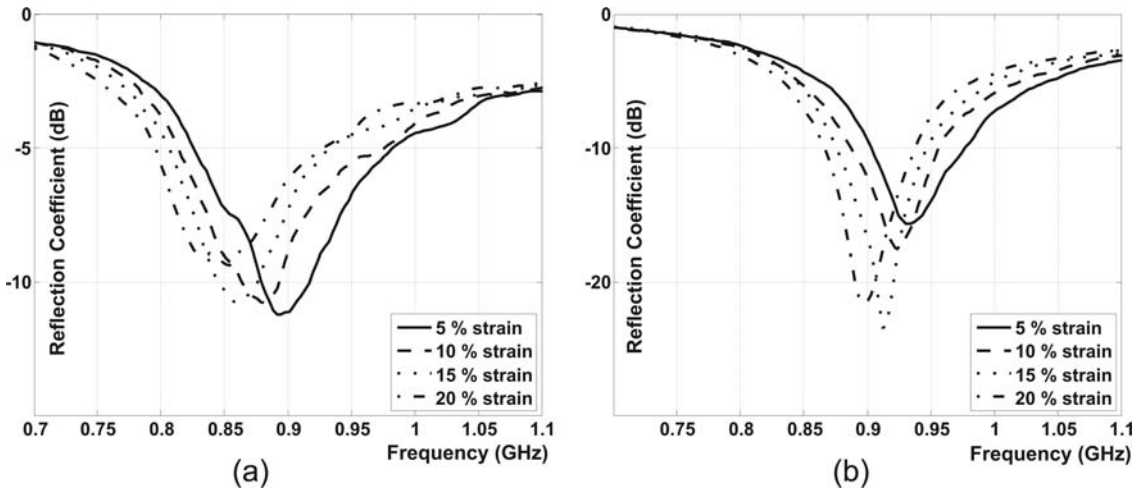

Fig. 4 Measured reflection coefficient of the strained antenna, with elongation along (a) *x*- and (b) *y*-axis. The corresponding coordinate system is shown in Fig. 3.

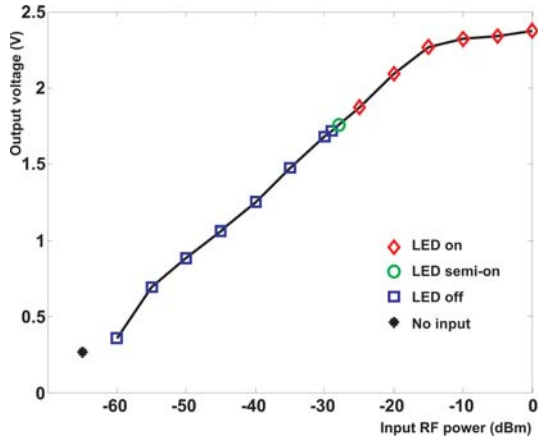

Fig. 5 Measured output DC voltages of the RF power detection sub-module and the LED on/off states *versus* varying input RF power.

the measured output DC voltages *versus* the varying input RF power ranging from −60 dBm to 0 dBm. In the case of no RF input, a DC voltage of 0.25 V was measured at the output port, which was clearly lower than that with −60 dBm input power. The experimental data in Fig. 5, show a linear behaviour when the RF input varies between −55 dBm and −15 dBm. This implies that the curve of the input RF power *versus* the corresponding output DC voltages can be easily interpolated based on a couple of measured points. It was found that the LED was switched to the semi-on state when its forward bias voltage reached 1.76 V. The LED completely turned on with a high light intensity if a higher bias voltage was applied. In the demonstrated RF power detection sub-module, the output voltage of 1.76 V corresponded to an RF input of −28 dBm. While the input RF power was above −28 dBm, the LED indicator remained in its on-state, and *vice versa*.

4.3 Integration and RF radiation detection demonstration

Various metallic materials for realizing reliable interconnects between FPCs and liquid alloy microfluidic antennas have been tested. Excellent wetting and very low contact angles between Galinstan and the surfaces of some solid metals like gold, tin and solder alloy were observed in the experiments.‡ Poor wettability of Galinstan on a copper or stainless steel surface was seen. Although its wettability could be improved to a certain degree by polishing the metal surface, it was still far away from that of the above mentioned metals. Aluminium is certainly not a good choice for interconnects, because it was dissolved in Galinstan. Therefore, tin-plated contact pins were chosen in the demonstrated prototype.

Fig. 6 shows photographs of the stretchable RF radiation sensor operating in ordinary office environment. The LED indicator of the sensor was on in the case of direct RF illumination. Stretching the integrated device up to 15% along either *x*- or *y*-axis did not cause any mechanical damages or failure in the RF radiation sensing. Additionally, the sensor could also tolerate

‡ The tests were conducted by digging various solid metal pins into the liquid metal and then pulling them out. Later, the residual liquid metal on each metallic pin was observed.

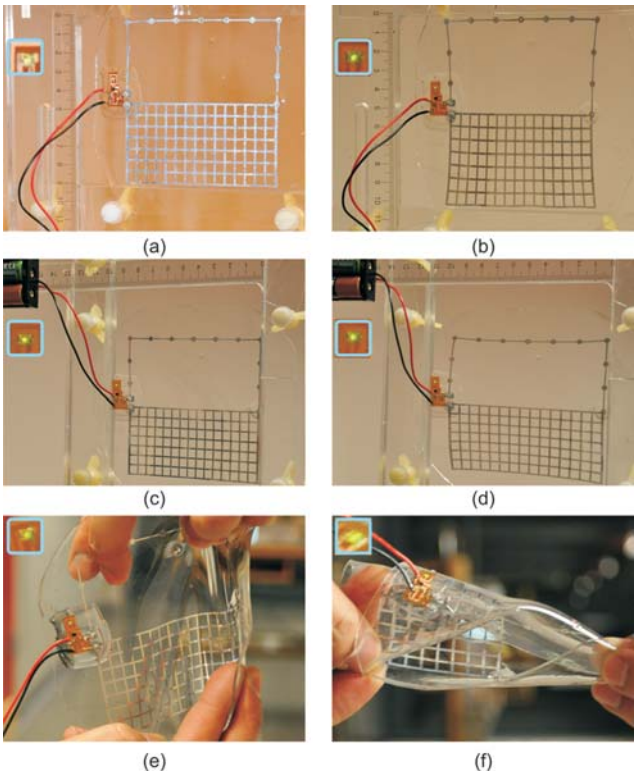

Fig. 6 Photographs of the stretchable RF radiation sensor operating in ordinary office environment: (a) and (c) non-stretched RF radiation sensor, (b) strained sensor with 15% elongation along *x*- and (d) *y*-axis, (e) sensor with manually applied strain in both *x* and *y* direction and (f) severe twisting. The sensor was directly illuminated by a radiation source placed 5 m away. The corresponding coordinate system is given in Fig. 3.

severe folding and twisting with maintained sensing functionality. When the sensor was directly illuminated by RF radiation, its LED indicator remained in the on-state regardless of straining, folding and twisting. It immediately turned off while the RF signal generator was switched off or the RF radiation was blocked by a human hand or body. The former case verified that the sensor was only sensitive to the radiation source in the demonstration setup than other radiation sources from the surroundings. The latter can be explained by significant attenuation of the human body of the RF signal around 900 MHz. Even if weak RF radiation penetrating through the human body or reflected by the surroundings could be detected by the radiation sensor, it was too low to drive the LED indicator. The detailed results are summarized in Table 2. To further verify the radiation sensing functionality, the same experiments were repeated in an anechoic chamber, in which no reflections or scatterings from the surroundings existed. The identical results were however achieved as presented in Table 2.

High stretchability up to 40% of the standalone stretchable antennas has been previously demonstrated. Due to the presence of the LSC, the presented elastic RF radiation sensor only exhibited stretchability up to 15%. A couple of feasible solutions can be employed to further improve the elasticity of integrated devices. For instance, utilizing further miniaturized ICs and passive components, directly embedding thinned bare IC dies in

Table 2 LED on/off states when the non-strained and strained sensor device was illuminated by a RF radiation source with a distance of 5 m. All the tests reported here were carried out in ordinary office environment[a]

Elongation	Orientation[b]	No shielding	Hand/body shielding
No strain	Horizontal	On	Off
	Vertical	On	Off
5% *x*-axis	Horizontal	On	Off
	Vertical	On	Off
10% *x*-axis	Horizontal	On	Off
	Vertical	On	Off
15% *x*-axis	Horizontal	On	Off
	Vertical	On	Off
5% *y*-axis	Horizontal	On	Off
	Vertical	On	Off
10% *y*-axis	Horizontal	On	Off
	Vertical	On	Off
15% *y*-axis	Horizontal	On	Off
	Vertical	On	Off
Manually applied strain in both *x* and *y* direction		On	Off
Folding		On	Off
Twisting		On	Off

[a] The presented results were obtained while the RF signal generator was on and transmitted CW signal at 900 MHz. Once the signal generator was switched off, the LED indicator turned off immediately. [b] The orientation is defined with respect to the *x*-axis of the stretchable unbalanced loop antenna. The corresponding coordinate system is depicted in Fig. 3.

flexible laminates, or implementing integrated passives based on flex foils.

The measured current consumption of the entire radiation sensor was 7.65 mA at a DC supply voltage of 5.23 V. This means that four serially connected AA Duracell 2650 mAh can drive the demonstrated sensor in a continuous sensing mode for more than 300 h. Of course, longer operational time can be achieved by programming the integrated device to a discontinuous sensing mode. Such additional functionality necessitates more complex circuits, *e.g.* microcontrollers or power management modules. Integration of power supply modules like thin film rechargeable batteries, energy harvesting units, or solar cells into stretchable electronic devices would be another interesting research topic. Nevertheless, significant amounts of efforts are needed for developing power supply modules with high degrees of stretchability and foldability.

5 Conclusions

The first elastic integrated RF electronic device has been presented in this article. The concept of incorporating FPCs to microfluidic elastic passive components exhibits a cost-effective solution for realizing high-performance stretchable ICs at radio frequencies. A stretchable RF radiation sensor based on the proposed concept has been demonstrated with good RF radiation detection sensitivity as well as severely mechanical deformability. Stretchability of integrated devices can be further enhanced in the future studies by utilizing advanced packaging or integration techniques and in-depth investigating the mechanism of non-stretchable and elastic structures. The merits such as easy prototyping and low cost manufacturing make the presented technique very attractive for various emerging applications, and thus stimulate considerable research and development activities in this field. It is anticipated that the further development of the proposed microfluidic stretchable RF electronics concept would enable more complex wireless communication and remote sensing devices with enhanced elasticity associated with increased functionality in the near future.

Acknowledgements

The authors thank Prof. Klas Hjort for his assistance with the access to the cleaning room facilities. This work was partially funded by INNOVATIONSBRON, Sweden, under the Fokus I program (Project No. 400694).

References

1 G. M. Whitesides, *Nature*, 2006, **442**, 368–373.
2 J. El-Ali, P. K. Songer and K. F. Jensen, *Nature*, 2006, **442**, 403–411.
3 P. S. Disttrich and A. Manz, *Nat. Rev. Drug Discovery*, 2006, **5**, 210–218.
4 A. Wu, L. Wang, E. Jensen, R. Mathies and B. Boser, *Lab Chip*, 2010, **10**, 519–521.
5 A. C. Siegel, S. S. Shevkoplyas, D. B. Weibel, D. A. Bruzewicz, A. W. Martinez and G. M. Whitesides, *Angew. Chem., Int. Ed.*, 2006, **45**, 6877–6882.
6 A. C. Siegel, D. A. Bruzewicz, D. B. Weibel and G. M. Whitesides, *Adv. Mater.*, 2007, **19**, 727–733.
7 H.-J. Kim, C. Son and B. Ziaie, *Appl. Phys. Lett.*, 2008, **92**, 011904.
8 H.-J. Kim, T. Maleki, P. Wei and B. Ziaie, *J. Microelectromech. Syst.*, 2009, **18**, 138–146.
9 S. Cheng, A. Rydberg, K. Hjort and Z. G. Wu, *Appl. Phys. Lett.*, 2009, **94**, 144103.
10 S. Cheng, Z. G. Wu, P. Hallbjorner, K. Hjort and A. Rydberg, *IEEE Trans. Antennas Propag.*, 2009, **57**, 3765–3771.
11 J. H. So, J. Thelen, A. Qusba, G. J. Hayes, G. Lazzi and M. D. Dickey, *Adv. Funct. Mater.*, 2009, **19**, 3632–3637.
12 J. A. Rogers, T. Someya and Y. Huang, *Science*, 2010, **327**, 1603–1607.
13 D.-H. Kim and J. A. Rogers, *Adv. Mater.*, 2008, **20**, 4887–4892.
14 Stella homepage. http://www.stella-project.de/ (accessed April 5th, 2010).
15 A. J. Baca, J.-H. Ahn, Y. G. Sun, M. A. Meitl, E. Menard, H.-S. Kim, W. M. Choi, D.-H. Kim, Y. Huang and J. A. Rogers, *Angew. Chem. Int. Edit.*, 2008, **47**, 170–188.
16 A. C. Arias, J. D. MacKenzie, I. MaCulloch, J. Rivnay and A. Salleo, *Chem. Rev.*, 2010, **110**, 3–24.
17 R. H. Reuss, B. R. Chalamala, A. Moussessian, J. A. Rogers, M. Hatalis, D. Temple, G. Moddel, B. J. Eliasson, M. J. Estes,

J. Kunze, E. S. Handy, E. S. Harmon, D. B. Salzman, J. M. Woodall, M. A. Alam, J. Y. Murthy, S. C. Jacobsen, M. Olivier, D. Markus, P. M. Campbell and E. Snow, *Proc. IEEE*, 2005, **93**, 1239–1256.
18 L. Gatzoulis and I. Iakovidis, *IEEE Eng. Med. Biol. Mag.*, 2007, **26**, 51.
19 D.-H. Kim, J.-H. Ahn, W. M. Choi, H.-S. Kim, T.-H. Kim, J. Z. Song, Y. Huang, Z. J. Liu, C. Lu and J. A. Rogers, *Science*, 2008, **320**, 507–511.
20 D. H. Kim, J. Z. Song, W. M. Choi, H. S. Kim, R. H. Kim, Z. J. Liu, Y. Y. Huang, K. C. Hwang, Y. W. Zhang and J. A. Rogers, *Proc. Natl. Acad. Sci. U. S. A.*, 2008, **105**, 18675–18680.
21 D.-H. Kim, Y.-S. Kim, J. Wu, Z. Liu, J. Song, H.-S. Kim, Y. Y. Huang, K.-C. Hwang and J. A. Rogers, *Adv. Mater.*, 2009, **21**, 3703–3707.
22 H. C. Ko, M. P. Stoykovich, J. Song, V. Malyarchuk, W. M. Choi, C.-J. Yu, J. B. Geddes, J. Xiao, S. Wang, Y. Huang and J. A. Rogers, *Nature*, 2008, **454**, 748–753.
23 J. Viventi, D.-H. Kim, J. D. Moss, Y.-S. Kim, J. A. Blanco, N. Annetta, A. Hicks, J. Xiao, Y. Huang, D. J. Callans, J. A. Rogers and B. Litt, *Sci. Transl. Med*, 2010, **2**, 24ra22.
24 S. P. Lacour, S. Wagner, Z. Y. Huang and Z. G. Suo, *Appl. Phys. Lett.*, 2003, **82**, 2404.
25 S. P. Lacour, J. Jones, S. Wagner, T. Li and Z. G. Suo, *Proc. IEEE*, 2005, **93**, 1459–1467.
26 D. Brosteaux, F. Axisa, M. Gonzalez and J. Vanfleteren, *IEEE Electron Device Lett.*, 2007, **28**, 552–524.
27 B. Huyghe, H. Rogier, J. Vanfleteren and F. Axisa, *IEEE Trans. Adv. Packag.*, 2008, **31**, 802–808.
28 R. Cartaa, P. Jouranda, B. Hermansa, J. Thonéa, D. Brosteauxb, T. Vervustb, F. Bossuytb, F. Axisab, J. Vanfleterenb and R. Puersa, *Sens. Actuators, A*, 2009, **156**, 79–87.
29 T. Sekitani, Y. Noguchi, K. Hata, T. Fukushima, T. Aida and T. Someya, *Science*, 2008, **321**, 1468–1472.
30 F. Scharmann, G. Cherkashinin, V. Breternitz, Ch. Knedlik, G. Hartung, Th. Weber and J. A. Schaefer, *Surf. Interface Anal.*, 2004, **36**, 981–985.
31 N. B. Morley, J. Burris, L. C. Cadwallader and M. D. Nornberg, *Rev. Sci. Instrum.*, 2008, **79**, 056107.
32 M. D. Dickey, R. C. Chiechi, R. J. Larsen, E. A. Weiss, D. A. Weitz and G. M. Whitesides, *Adv. Funct. Mater.*, 2008, **18**, 1097–1104.

